New York University
School of Engineering and Science
Research Division

Investigation of the Effect of Pressure on Metallurgical Phenomena

Final Report

20 June 1960 to 30 September 1965

on

Research Grant NsG 90-60

by

H. Margolin
I. Cadoff
B. Siegel
E. Pan

to

National Aeronautics and Space Administration
Washington, D. C.

TABLE OF CONTENTS

Investigation of the Effect of Pressure on Metallurgical Phenomana

Phase A

I. Introduction

High pressure studies on thallium and thallium alloys (1), indicate that thallium can exist in the close-packed-hexagonal structure, the body-centered-cubic structure, and the face-centered-cubic structure. At atmospheric pressure, pure thallium can only exist in the c.p.h. and b.c.c. forms. At elevated pressures, however, the f.c.c. structure is stable.

The addition of substitutional lead to pure thallium results in a f.c.c. structure at atmospheric pressure. It is desireable to find out whether or not the f.c.c. alloy phase at atmospheric pressure, and the pure thallium f.c.c. phase at elevated pressures are both part of the same continuous region in P-T-X space. Such information could be determined by high pressure experiments, assuming the atmospheric pressure binary phase diagram was known.

Having analyzed the data in the literature, Hansen (2) has presented the thallium-lead atmospheric-pressure isobaric phase-diagram. He has noted that much of the data concerning solid-solid equilibria is questionable. The majority of the investigations carried out were performed prior to 1940. The purity of the thallium used was therefore poor according to present standards. For these reasons, the phase diagram in Hansen, specifically the thallium-rich portion, could not be accepted as well defined. Therefore, prior to any high-pressure experiments, the atmospheric pressure phase diagram was re-investigated at the thallium rich end.

II. Experimental Procedure

A. Preparation of Alloys

The thallium used in this investigation was obtained from the American Smelting and Refining Company. All samples used were from lot #16, and had a purity of 99.999+% thallium. The material arrived as individually wrapped samples of approximately 25 grams. Each such slug was coated by the supplier with a protective fluid in order to prevent oxidation of the thallium.

On preparing an alloy, one slug was washed in a solution of one part sulphuric acid to one part distilled water. This was done in order to

remove any surface dirt, as well as to remove the protective fluid. The specimen was then transferred to a beaker containing distilled water. Thallium is insoluble in water, but thallium oxide is soluble in water. Thus, rinsing in distilled water removed not only sulfate, but oxide as well.

The sample was dried with absorbent paper and rinsed again in distilled water. This process was repeated three to four times. After the last rinse, the specimen was placed into a weighing bottle which contained ethelyne glycol. This fluid prevented the oxidation of the thallium, but dissolved thallium at a very slow rate (see section on storage of alloys). The weighing bottle containing ethelyne glycol was weighed with and without the thallium specimen. The apparent weight of the specimen was determined by difference. The true weight of the specimen was determined by correcting the apparent weight for the buoyancy effect of ethelyne glycol.

The lead used was obtained from the J. T. Baker Chemical Company, Phillipsburg, New Jersey. The lead used was from lot #29286, and was 99.996% pure. The impurities are shown in Table I.

The weighed thallium sample, and the necessary amount of lead were placed in a vycor tube with an outside diameter of 13 millimeters. The thallium still had a thin coat of the ethelyne glycol on the surface to prevent oxidation during handling. The tube was then evacuated to less than .5 microns, which was a sufficiently low pressure to volatalize and remove the ethelyne glycol. The capsule was then flushed with argon, re-evacuated, flushed again with argon and re-evacuated a second time to a vacuum of less than .5 microns. Argon was then introduced into the system, to a pressure slightly less than one atmosphere, and the capsule was sealed. All capsules were checked for leakage with a Tesla coil.

The capsule containing the thallium and lead was heated to 350°C. for twenty minutes, removed from the furnace, agitated, and re-heated. This procedure was followed three times. After the third agitation, the capsule was quickly immersed into a bath containing acetone and dry ice.

The capsule, after cooling, was immersed in a bath of ethelyne glycol, and broken. The slug of alloy was then hammered to close the pipe formed during the quench. The hammered specimen was rolled and hand drawn through a die into a wire of .038 inches in diameter. The wires were then re-capsuled and heat treated for twenty-four hours at 100°C., in order to assure homogeneity. During all of the above forming processes, ethelyne glycol was employed as the lubricant and oxidation-preventer. Twenty-five alloys ranging from one to forty atomic per cent lead were made. The nominal compositions are shown in Table II.

B. Storage of Alloys

Adler (1) found that storing thallium in ethelyne glycol, at room temperature, for a few months, had no detectable effect on alloy composition. However, after storage for times greater than six months, alloy compositions changed, due to solution of thallium in the ethelyne glycol. To prevent any significant change in composition, the alloys were stored in ethelyne glycol, but at dry ice temperatures. At these temperatures, the ethelyne glycol solidified, and the alloy wires were imbedded in the solid ethelyne glycol. Thus, the tendency for solution of the thallium in the ethelyne glycol was reduced, and no detectable effect on the weight of the wires was found to about one part in 250.

C. Resistivity Apparatus

To determine the electrical resistance (r) of the specimens, the specimens were connected in series with a six volt battery and another resistor whose resistance was determined.

The resistance of the standard resistor was determined with a low resistance bridge. Currents of 1/2, 1, and 2 amperes were passed through the carbon resistor, and the electrical resistance was measured with the bridge. Three such determinations were made at each current level. The resistance was determined to be .1005 ohms. No deviation from this value was detected in any of the nine readings made. The standard resistor was then placed in a cardboard box, (6"x3"x1") surrounded by insulation, and wrapped in aluminum foil. Four wires were connected to the resistor; two for potential leads, and two for current leads.

Nichrome wire was coiled, and wrapped similar to the standard resistor. Approximately six ohms of wire was used. This wire was connected in series with the rest of the circuit, in order to decrease the current drawn by the circuit. With this resistance in the circuit, the circuit drew about one ampere of current.

Both the nichrome and the standard resistor were wrapped carefully in order to prevent temperature fluctuations during a run. Such fluctuations in temperature can cause resistance changes, and thus cause a fluctuating current.

The thallium-lead alloys, in wire form, were connected in series in the circuit, and two potential leads were tapped. These wires, however, are very soft, and a technique was needed to keep the wire straight. Figure 1 shows the wire specimen in the four point probe used in this investigation. The specimen was placed in a thick-walled glass tube, whose inside diameter was .060 inches. Two flat copper sheets, with .040 inch diameter holes in their centers, were used as the potential leads. The copper sheets were held rigid, and electrically insulated from each other by two threaded teflon screws. The ends of the wire specimens were connected to the rest of the circuit with crimp connectors.

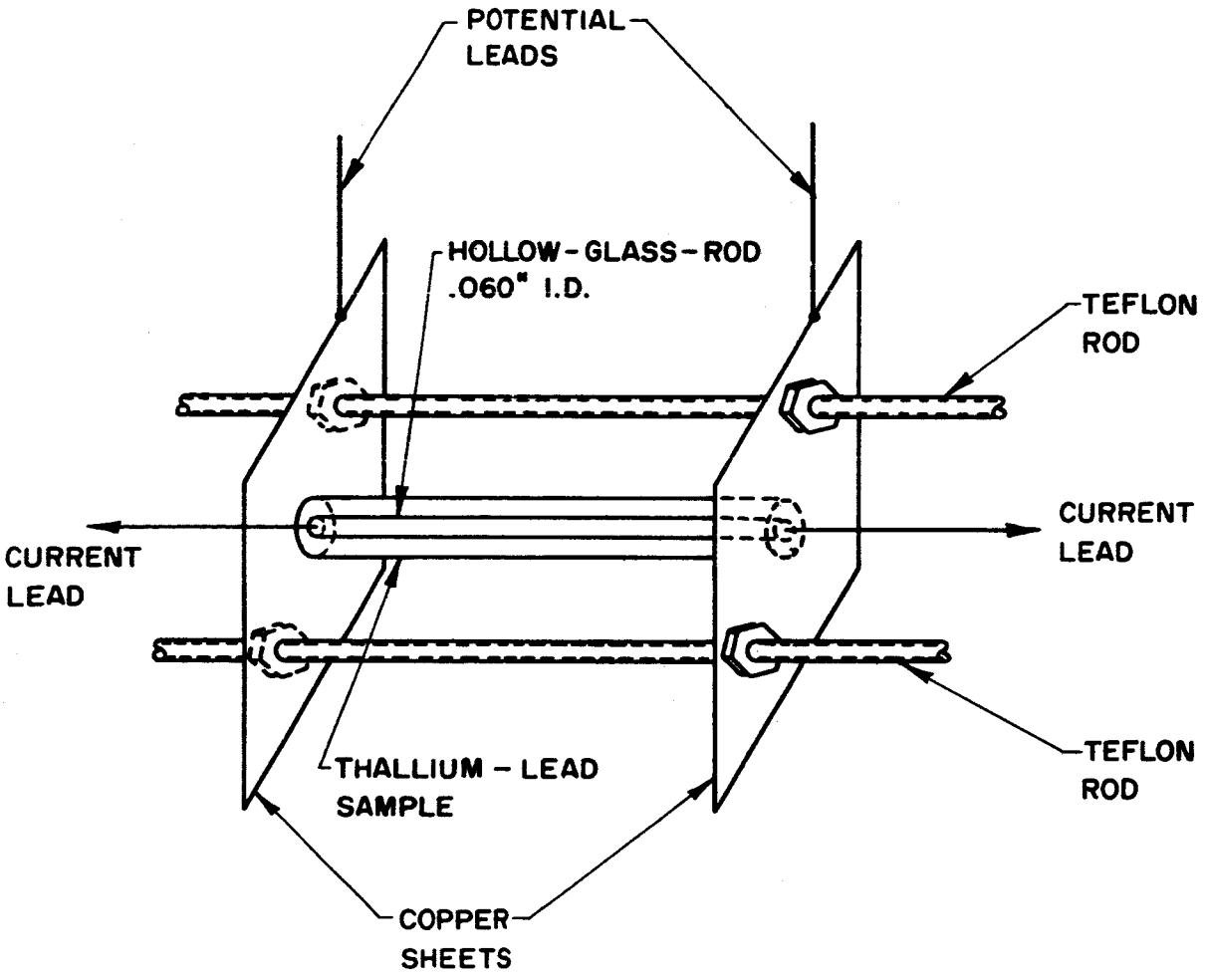

Fig. 1. Resistivity apparatus.

The specimen was immersed in a bath of Canthus 210 oil provided by the Esso Company. The temperature of the bath was controlled with two heating coils. One coil yielded about 500 watts, the other 1000 watts. The temperature was kept uniform by agitating the oil with a heavy-duty electrical stirrer. Temperature was measured with partial-immersion thermometers. The resistivity was measured as a function of temperature by making runs while heating the system and while cooling the system. However, the majority of runs were made while heating the system.

The two heaters were connected to variable resistors, so that they could be run at any fractional part of their rated power. Thus, by changing the setting on the variable resistor, different heating and cooling rates were produced. Preliminary runs were made in which the heating rate was 40°C per hour. However, runs were later made in which the heating rate was reduced to only 12°C per hour. In some instances, the variable resistors were set so that the temperature was held constant for 5-30 minutes.

The oil bath served a dual purpose. First, it maintained a uniform temperature, and second, it prevented oxidation of the thallium-lead alloys. The results of the run of the pure thallium specimen agreed with the results of a run on pure thallium which was sealed in an evacuated pyrex bulb.

By measuring the voltage drop across the standard resistance, and across the alloy specimen, the electrical resistance of the sample could be determined. In order to determine the specific resistance or resistivity of the specimen, however, the length and cross-sectional area of the wire had to be measured. These measurements were made with micrometers. The voltage drops were measured with a Leeds-Northrop Millivolt Potentiometer, capable of differentiating .01 mv.

D. X-Ray Investigations

Powder patterns of various alloys were made using a Debye-Scherrer camera. However, due to the high susceptibility to oxidation, wire samples were used instead of powder samples. These specimens were sealed in a quartz capillary, under vacuum. Copper radiation was used- filtered by nickel foil of .001 inch thickness. The film was surrounded by aluminum foil of .004 inch thickness in order to reduce the effect of the fluorescent radiation. Exposure times of 16 to 20 hours were used. The X-ray unit was run at 35,000 volts and 20 milli-amperes.

It was found necessary to age the samples at least twenty-four hours after preparation, in order to obtain sharp lines. With no aging process, the lines were broad.

Alloy samples were X-rayed at elevated temperatures as well. The samples for high temperature X-ray experiments were prepared similiar to

the low temperature method. Because the transformation from the high temperature phases to the low temperature phases was found to be extremely sluggish, X-ray patterns were taken in order of ascending temperatures. Patterns were taken at 140, 160, 240, and 260°C. The furnace used in conjunction with the high temperature Jarrell-Ash Camera was calibrated and the temperature of the specimen vs. the controller setting was determined. the accuracy was ± 3°C.

III. Results and Conclusions

A. Resistivity Data

The resistivity of the thallium-lead alloys was found to increase linearly with temperature, up to a point where some of the alloys exhibited a drop in resistivity upon increasing temperature. This drop was attributed to crossing a phase boundary.

Runs which were carried out on cooling gave different temperatures of the discontinuity as a function of cooling rate. The faster the cooling rate, the lower the discontinuity temperature. The reaction in the four and five per cent alloys was so sluggish that the discontinuity on cooling was never observed. This indicated that the high temperature phase was retained, even down to room temperature. This observation and interpretation might explain the reported stability of the b.c.c. structure in thallium-lead alloys at room temperature (3).

On heating, however, the temperature of the discontinuity was, within experimental error, not a function of the heating rate. To insure equilibrium conditions, preliminary runs were made with heating rates in the order of 40°C per hour. These runs were made in order to determine roughly the location of the resistivity discontinuity. Subsequent runs were made with heating rates in the order of 12°C per hour up to a few degrees below the discontinuity temperature. At this point the temperature was held constant for 15 minutes, in order to insure equilibrium. The temperature was then increased one to two degrees, and held constant. The temperatures of the discontinuities observed in various alloys, and the phase boundaries corresponding to these discontinuities are given in Table III.

A typical resistivity vs. temperature plot for an alloy undergoing the $\alpha \rightarrow \alpha+\beta$ transformation is shown in Fig. 2. The first departure from the linear increase in resistivity occurred at 140°C. At this point the lower temperature linear curve melts another linear curve of different slope. This is indicative of passing from the $\alpha+\gamma$ region to the single phase α region. At a still higher temperature, the resistivity exhibited a decrease upon increasing temperature. This was indicative of the $\alpha \rightarrow \alpha+\beta$ transformation. When the reaction was complete, the resistivity continued to increase linearly with increasing temperature.

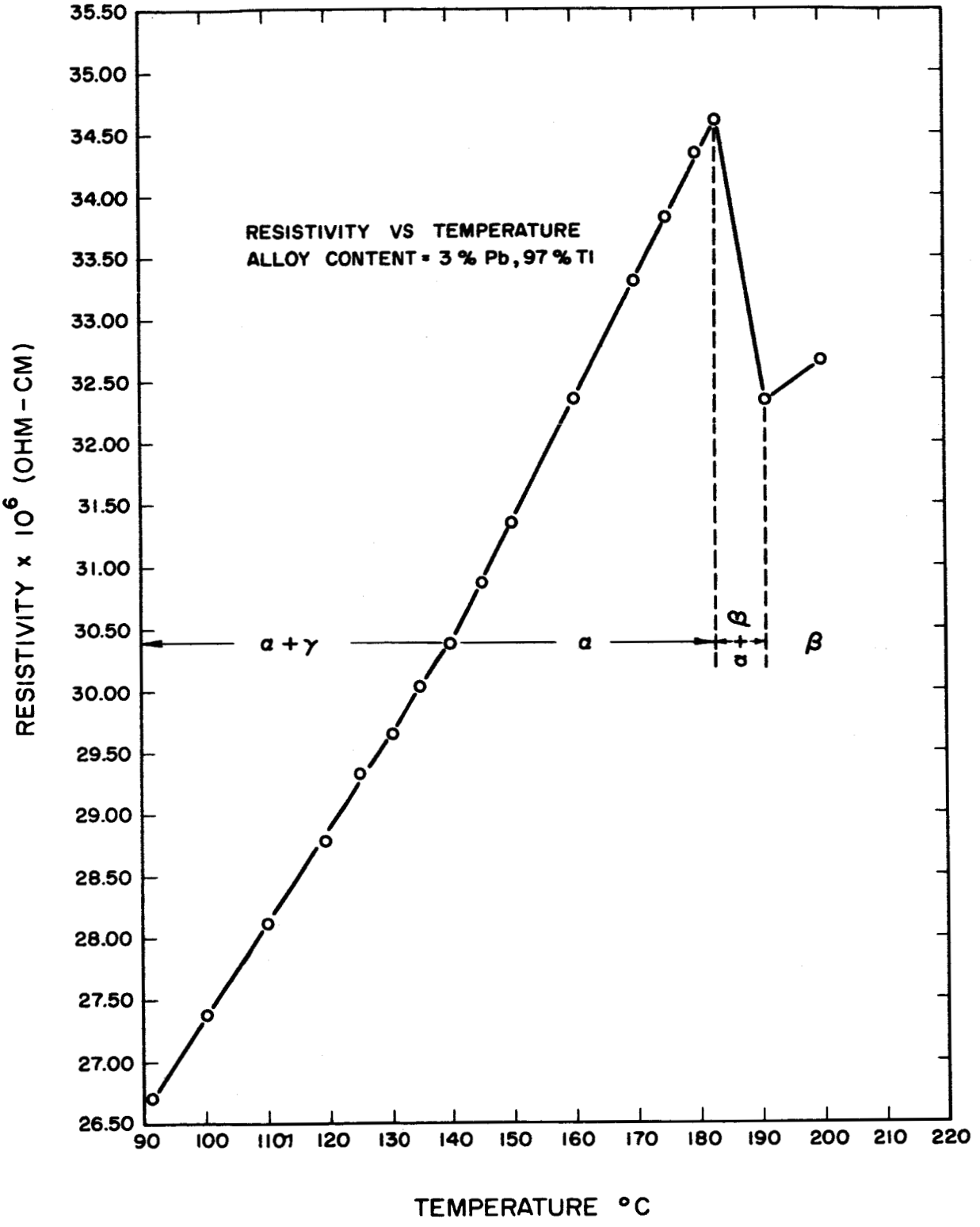

Fig. 2. Resistivity vs. temperature behavior for the 3.0% lead alloy.

Fig. 3 is a typical resistivity vs. temperature plot for an alloy in the hyper-eutectoid region. The drop in resistivity for these alloys is small in comparison to the hypo-eutectoid alloys. Note also that the drop occurs over a small temperature range of 2-3 degrees. The temperature of the discontinuity is constant for all the hyper-eutectoid alloys; this being the eutectoid temperature. The observation that a drop occurs in the resistivity vs. temperature curve, of hyper-eutectoid alloys, on heating past the eutectoid temperature is indicative of the fact that the resistivity of the f.c.c. phase is lower than the resistivity of the h.c.p. phase, at the same temperature. This conclusion is also substantiated by the resistivity isotherms.

The second discontinuity of the hyper-eutectoid alloys is due to the end of the eutectoid transformation. A small amount of superheating is necessary to transform completely to the high temperature phases. The second discontinuity, for hyper-eutectoid alloys, is therefore not indicative of crossing another phase boundary.

Specimens whose nominal composition ranged from 4 to 10 atomic per cent lead exhibit the same basic resistivity behavior as indicated by Fig. 3. The resistivity of alloys whose nominal composition were greater than 10% lead increased lineraly with temperature, and exhibited no discontinuities at the eutectoid temperature (180°C). The 11% alloy did however show a change in slope at 205°C. The resistivity increased linearly above this temperature, but at a different rate than at temperatures below 205°C. The temperature of 205°C then represents a point on the $\gamma/\beta+\gamma$ boundary. The data for the 11% alloy are plotted in Fig. 4.

B. Resistivity Isotherms

Plots were made at three temperatures of the resistivity as a function of composition. The temperatures were 140, 180, and 200°C. The results of these plots are shown in Fig. 5, and the data summarized in Table IV.

Fig. 5 shows that the addition of lead to pure thallium increases the resistivity until the maximum solubility of lead in pure thallium is reached. Additional lead content decreases the resistivity because it produces more γ, whose resistivity is lower than that of α. At 140 and 180°C, where only the α and γ exist, the resistivity decreases throughout the $\alpha+\gamma$ two-phase region. Further additions of lead to the β phase increase the resistivity. According to the data of Guertler and Schulze (4), this increase in resistivity goes through a maximum and then decreases continuously up to and including pure lead. The maximum in resistivity was not observed in this investigation because experiments were not run on alloys of high enough lead content.

The isothermal plot at 200°C. indicates the presence of five different phase fields at this temperature. Starting from pure thallium they are α, $\alpha+\beta$, β, $\alpha+\gamma$ and γ extending from about 10.9 per cent lead up to pure lead.

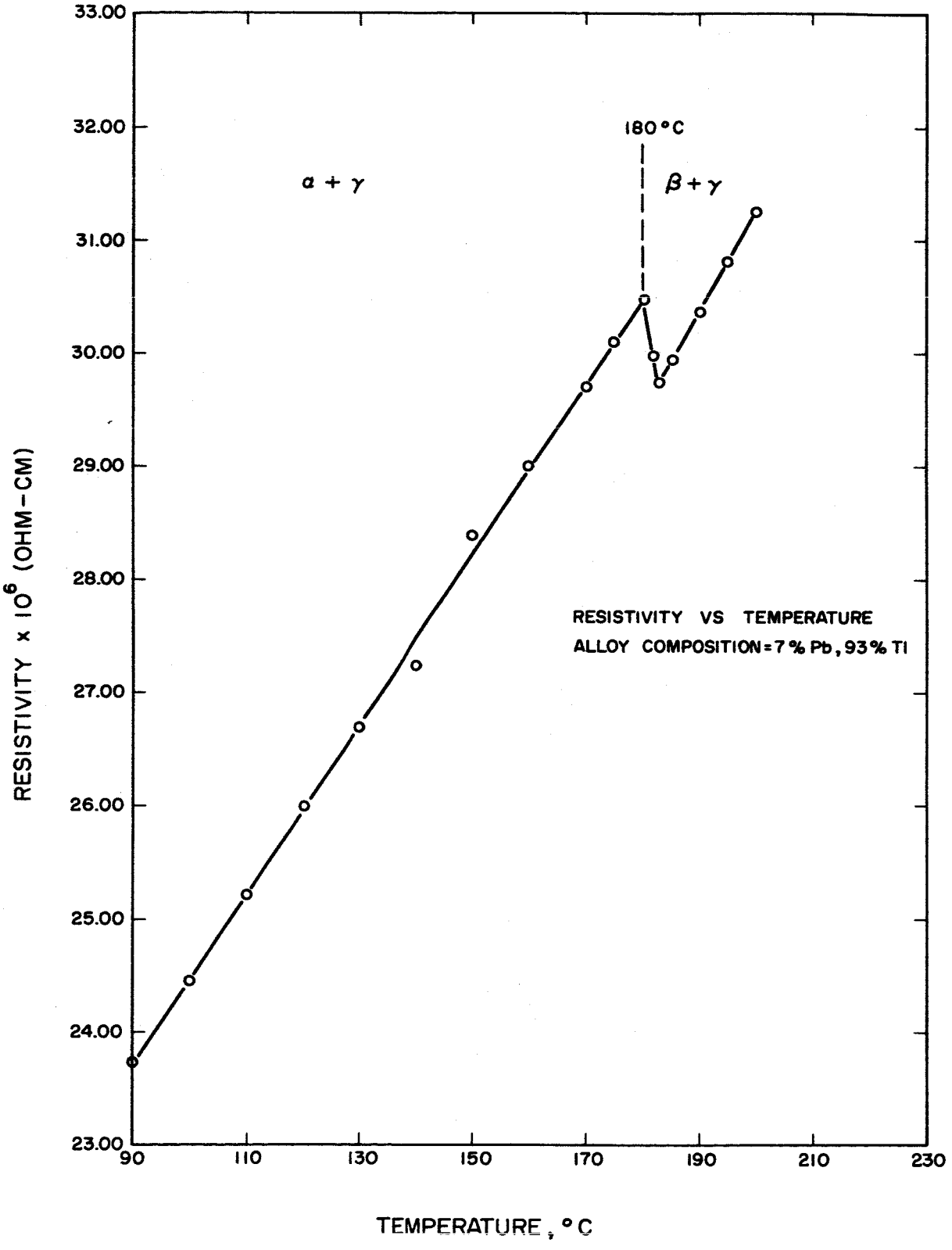

Fig. 3. Resistivity vs. temperature behavior for an alloy undergoing the eutectoid transformation.

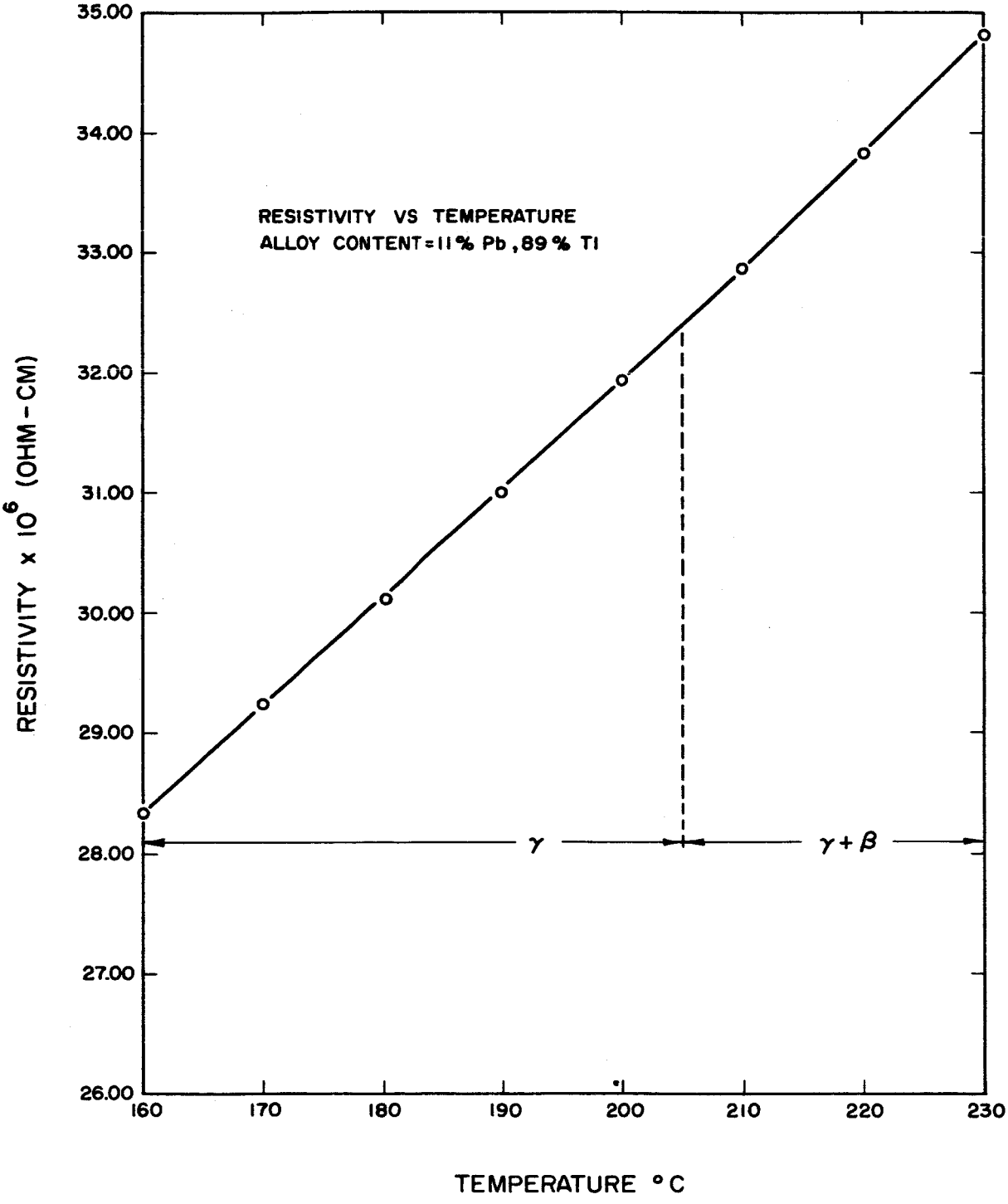

Fig. 4. Resistivity vs. temperature behavior for the 11.0% lead alloy.

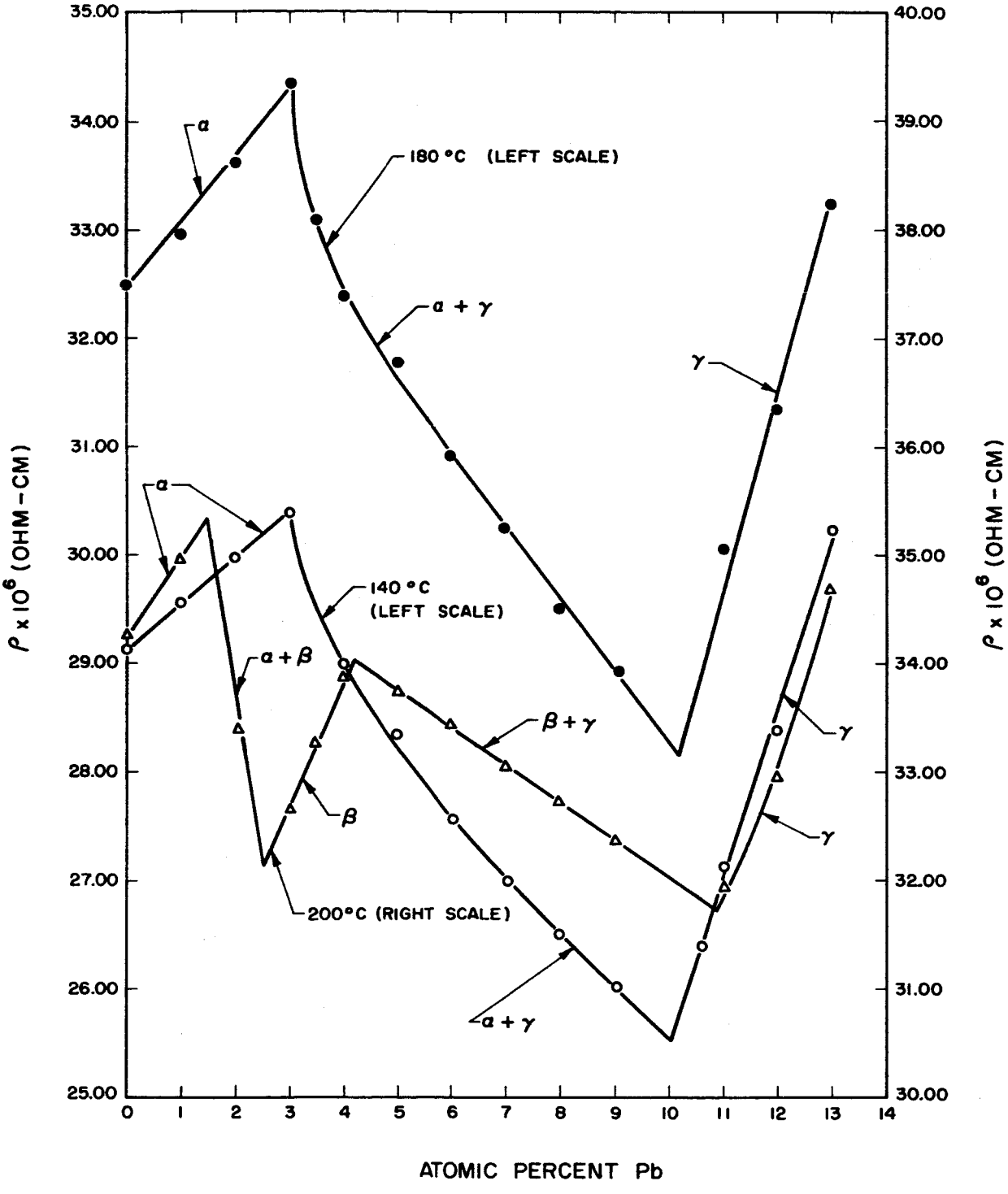

Fig. 5. Resistivity isotherms.

C. X-Ray Results

In order to check the resistivity results on the solubilities of lead in thallium and thallium in lead, and to determine the dolubilities above the eutectoid temperature, X-ray diffraction patterns were taken of several alloys, and the phases present were determined. Lattice parameter measurements were also computed from the results.

Fig. 6 is a plot of the lattice parameter of the f.c.c. phase as a function of composition at room temperature. Note that the lattice parameter of the γ phase is constant below 12.5%, but changes above 12.5% lead. Tang and Pauling did similar work (5), and arrived at the same result for the solubility of thallium in lead. The lattice parameter of the α phase was found to be constant above the composition of 2.8% lead.

D. Discussion

The data obtained from the curves of resistivity vs. temperature, resistivity vs. composition (isothermal), and lattice parameter vs. composition are plotted in Fig. 7. Although the topology of Fig. 7 is in agreement with the diagram drawn by Hansen (2), the actual position of the boundaries is not in agreement. Guertler and Schulze concluded that an eutectoid reaction occurs at 140°C. Their eutectoid horizontal extends from 6-20 per cent lead. However, their resistivity vs. temperature data in this composition range did not exhibit any discontinuities or slope changes. In this investigation, the eutectoid temperature was determined to be 180°C, and the eutectoid horizontal extended from about 3.2 to about 10.5% lead. All alloys in this range exhibited discontinuities at 180°C.

Guertler and Schulze constructed isotherms using their resistivity data, and determined the solubility of lead in thallium to be about 5.5-6.0% lead. However, Hansen noted that the solubility has been well established at about 3% lead, in fine agreement with the results of this investigation.

Fig. 8 shows the entire phase diagram proposed by the authors, using the data of the liquidus and solidus accepted by Hansen.

IV. Thermodynamic Calculations

The initial slope of the $\alpha/\alpha+\beta$ boundary, $\frac{\partial T}{\partial X}$, can be used to calculate the enthalpy change of the reaction $\alpha \rightarrow \beta$. According to Fig. 7, this slope would be 214/.056. The enthalpy change ΔH, is therefore:

$$\Delta H = -RT^2 / \frac{\partial T}{\partial X} \qquad (1)$$

Upon substitution, ΔH is calculated to be 133 cal/g-mole. This is in fairly good agreement with the various experimental values cited by Anderson et al. (6).

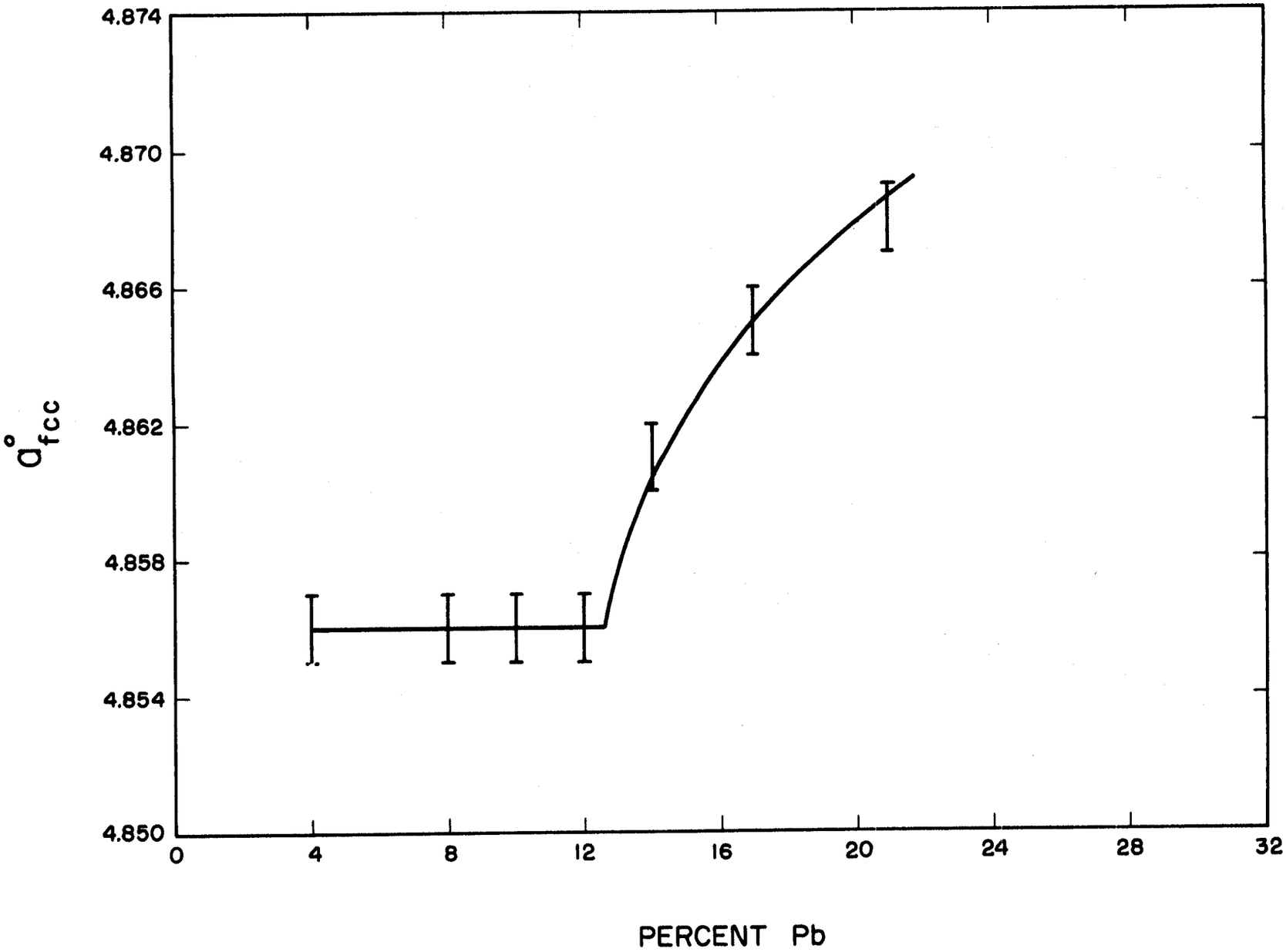

Fig. 6. Lattice parameter of the f.c.c. phase at room temperature.

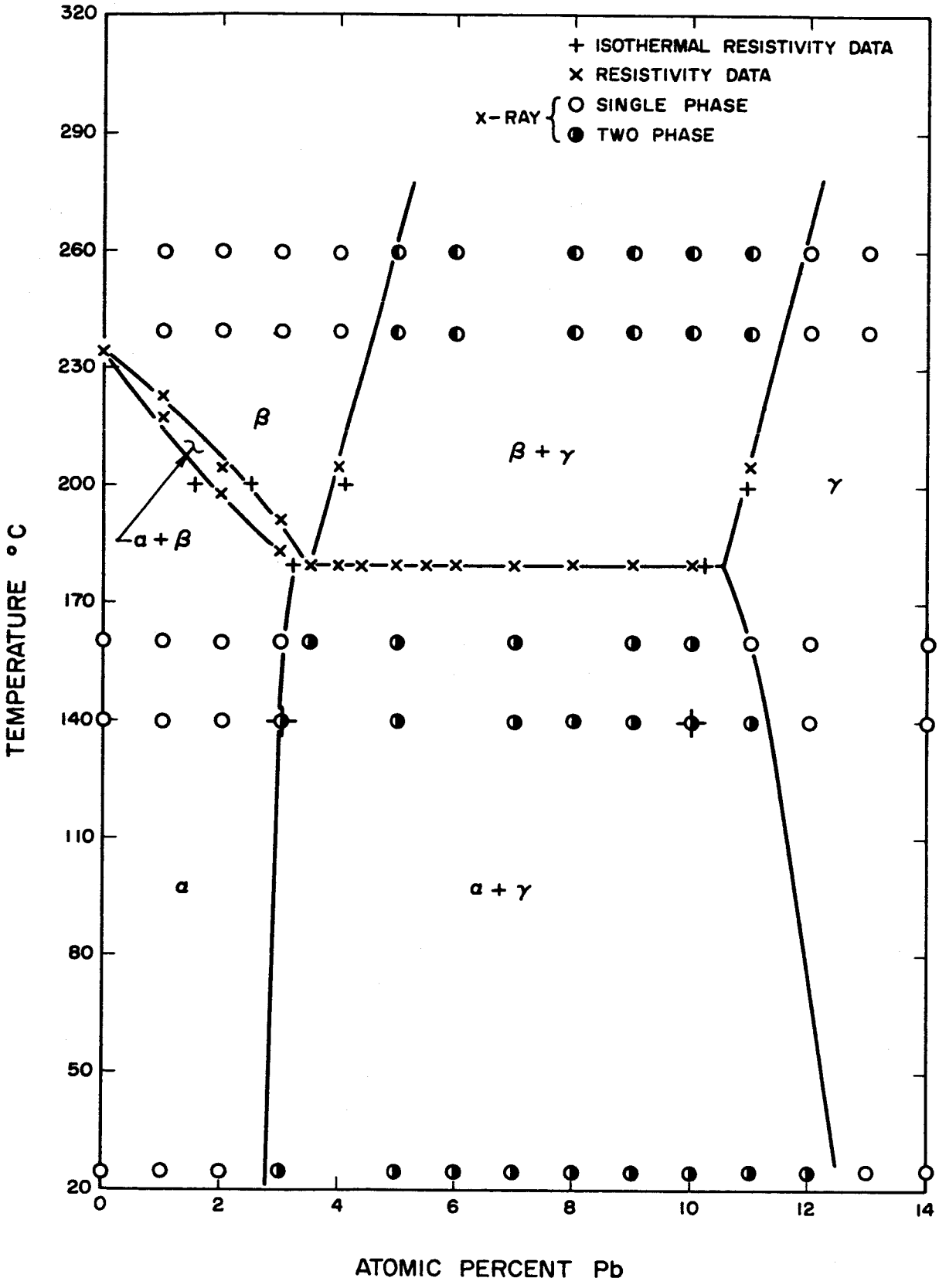

Fig. 7. The thallium rich portion of the thallium-lead phase diagram.

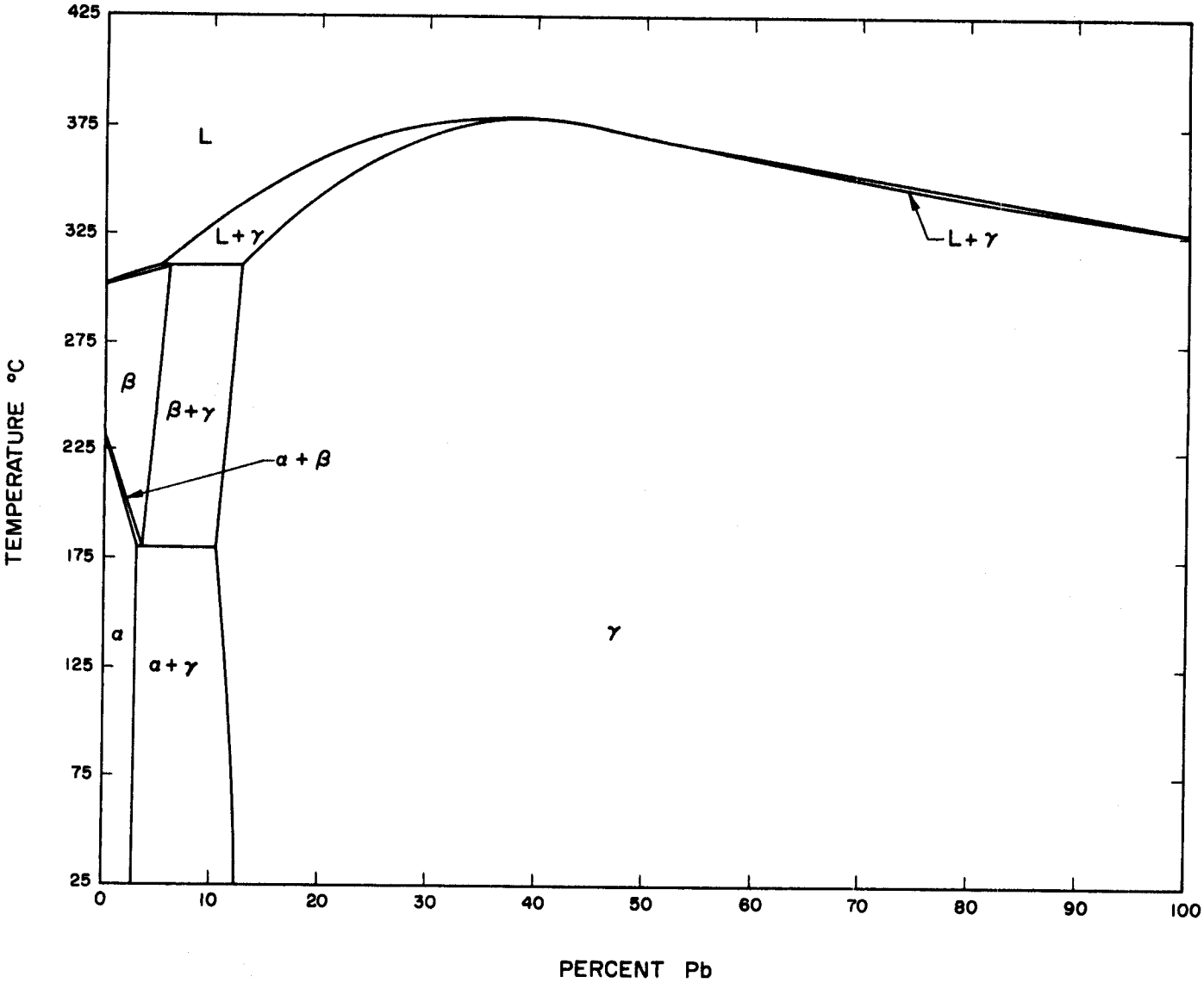

Fig. 8. The thallium-lead phase diagram.

For small amounts of solid solubility, the width of the $\alpha+\beta$ two-phase region can be calculated from the following equation.

$$\frac{\Delta T \, \Delta H}{RT^2} = -\Delta X \qquad (2)$$

If we use the accepted value of 90 cal/g-mole for the enthalpy of the reaction of pure thallium, and consider the temperature of 200°C, then equation 2 becomes

$$\Delta X = 90.34/(1.98.\ 473^2)$$

$$\Delta X = .007$$

This value is in excellent agreement with the experimental value obtained from Fig. 7.

V. Bibliography

1. Adler, P.: Doctoral Thesis, N.Y.U., 1964.

2. Hansen, M.: Constitution of Binary Alloys, Second Edition, P. 9, 1113-1116 McGraw Hill 1958.

3. Goldschmidt, V. M.: Z. Physik. Chem. Vol. 133, P. 9 490-410, 1928.

4. Guertler, W. and Schulze, A.: Z. Phsik. Chem. Vol. 104 269-309, 1923.

5. Tang, Y. and Pauling, L.: Acta Cryt. Vol. 5, 39-44, 1952.

6. Hultgren, R., Orr, R. L., Anderson, P. D. and Kelley, K. K.: Selected Values of Thermodynamic Properties of Metals and Alloys. 289-294 John Wiley and Sons, 1963.

Table I

Impurities present in the lead used in this investigation

Impurity element	weight per cent
Antimony and Tin	0.003
Arsenic	0.00003
Bismuth	0.0001
Copper	0.00005
Iron	0.00003
Nickel	0.00005
Silver	0.0002
Lead (by difference)	99.996

Table II

Nominal Compositions of Thallium-Lead Alloys

1.0	4.4	8.0	13.0	21.0
2.0	5.0	9.0	14.0	23.0
3.0	5.5	10.0	15.0	25.0
3.5	6.0	11.0	17.0	30.0
4.0	7.0	12.0	19.0	40.0

Table III

Phase Boundaries Determined From Resistivity Data

Nominal Composition (Atomic % Pb)	$\alpha+\gamma/\alpha$	$\alpha/\alpha+\beta$	$\alpha+\beta/\beta$	Eutectoid Temp	$\gamma/\gamma+\beta$	$\beta+\gamma/\beta$
0.0		235	235			
1.0		220	223			
2.0		198	202			
3.0	140	183	191			
3.5				180		
4.0				181		205
4.4				180		
5.0				180		
5.5				181		
6.0				180		
7.0				181		
8.0				180		
9.0				180		
10.0				180		
11.0					205	
12.0						
13.0						
15.0						

Table IV

Phases Observed By X-Ray Diffraction Techniques

Alloy Composition (atomic % lead)	Room Temp.	140°C	160°C	240°C	260°C
0.0	α	α	α		
1.0	α	α	α	β	β
2.0	α	α	α	β	β
3.0	α+γ	α+γ	α	β	β
3.5	α+γ		α+γ		
4.0				β	β
5.0	α+γ	α+γ	α+γ	β+γ	β+γ
6.0	α+γ			β+γ	β+γ
7.0	α+γ	α+γ	α+γ		
8.0	α+γ	α+γ		β+γ	β+γ
9.0	α+γ	α+γ	α+γ	β+γ	β+γ
10.0	α+γ	α+γ	α+γ	β+γ	β+γ
11.0	α+γ	α+γ	γ	β+γ	β+γ
12.0	α+γ	γ	γ	γ	γ
13.0	γ			γ	γ
14.0	γ	γ	γ		

High Pressure Effect on SnTe and PbTe

Phase B

I. Introduction

Electrical resistance and Seebeck coefficient of SnTe have been measured at constant pressure as a function of temperature and at constant temperatures as a function of pressure. The temperature range was from room temperature to about 400°C. The pressure range was from atmospheric pressure to about 35 kilobars. The data yielded a pressure-temperature phase diagram of SnTe in the solid state. Evidence for new solid phase of SnTe(III) at elevated temperature and high pressure has been observed. From thermodynamic considerations, a solid phase of SnTe(IV) has been postulated between SnTe(I) (room temperature and atmospheric pressure phase), SnTe(II) (room temperature and high pressure phase) and SnTe(III).

SnTe(III) showed semiconductor behavior in the resistivity measurements, with an energy gap of .28ev at 32 kilobars. The effect of pressure on the energy gap has been determined as $dEg/dP = 7.75 \times 10^{-6}$ ev/atm in the pressure range of 28 to 32 kilobars.

Electrical resistance and Seebeck coefficient of PbTe have been measured at constant pressures as a function of temperature. The data yield a $\frac{dE}{dP} = -7.65 \times 10^{-6}$ ev/atm.

II. Experimental Procedure

The crystals were prepared from 99.999% purity Pb, Sn and Te and were grown by a standard Bridgman technique. Cross sectional discs were cut from the crystal. These discs were assumed to have uniform carrier density. Long strips cut from the discs gave parallelopiped specimens. SnTe samples had $p_{300} = 1.7 \times 10^{20} cm^{-3}$ to $p_{300} = 3.83 \times 10^{20}$ carrier densities at 300°K, determined from Hall effect measurements. All the as grown PbTe single crystals had p-type carriers. N-type PbTe was obtained by heat treating p-PbTe at 775°C for about two days with a 5 atomic % excess Pb-PbTe two phase charge.

High pressure was obtained by utilizing a tetrahedral type high pressure apparatus. The high pressure tetrahedral cell design is shown in Figure 1. Figure 1a shows the assembled lava tetrahedron BCDE and also shows the two chromel-alumel thermocouples coming out from the edges of the tetrahedron. Figure 1b shows a cross sectional view ABC of the tetrahedron BCDE: "a" is a lava end piece; "b" is a boron nitride plug; "c" is molybdenum

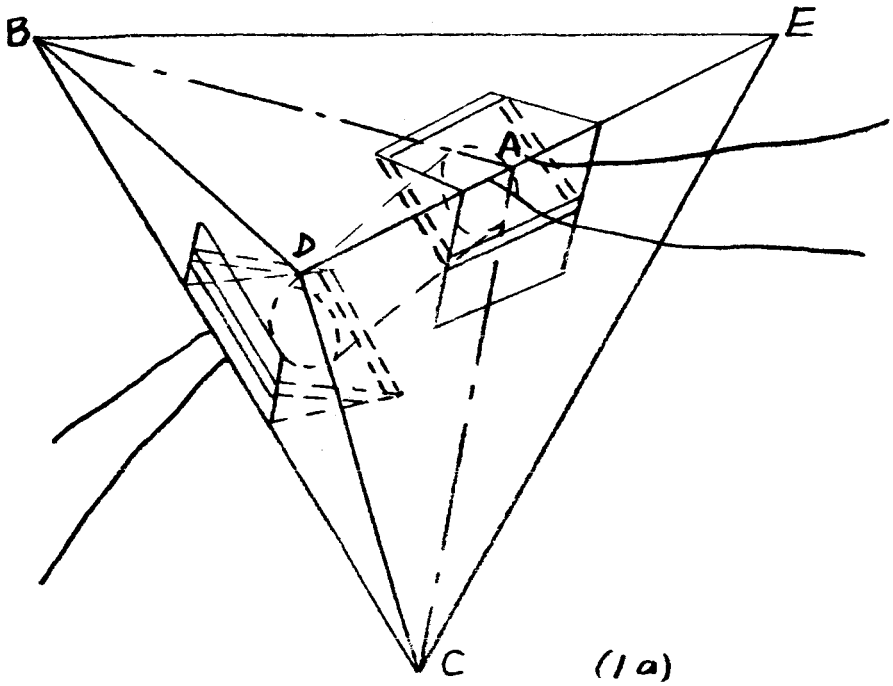

(1a)

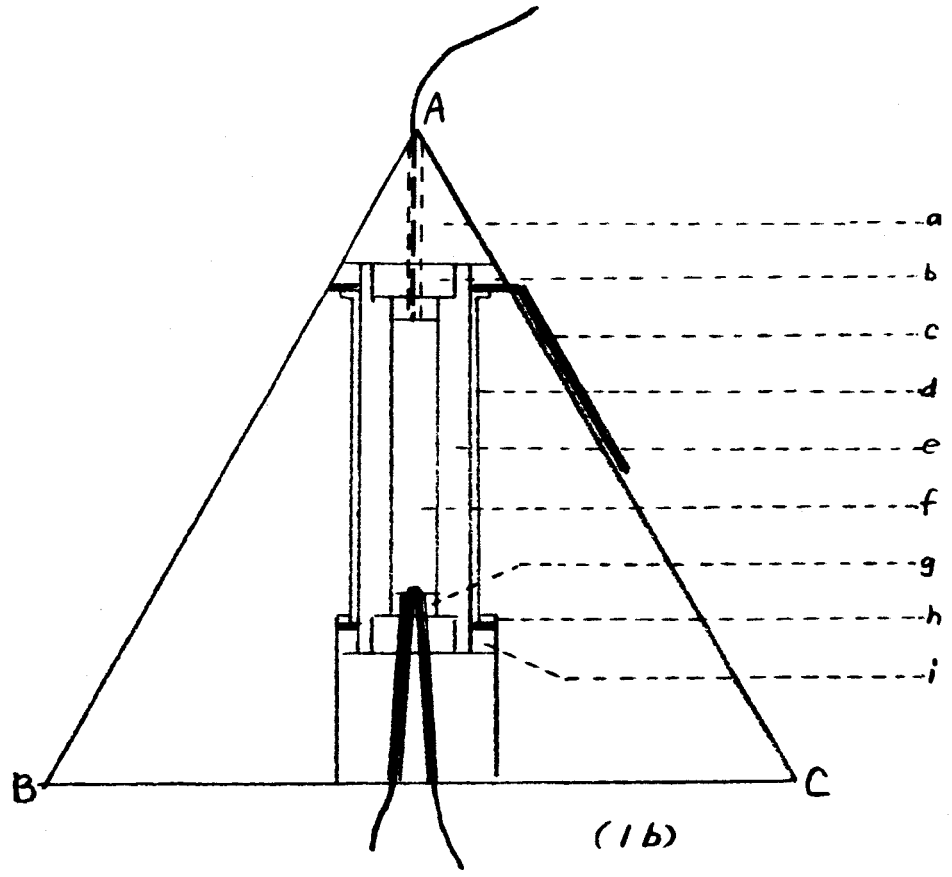

(1b)

Figure 1 High Pressure Tetrahedral Cell

sheet; "d" is the graphite furnace; "e" is a boron nitride specimen holder; "f" is the specimen; "g" is a brass plug; "h" is a steel ring; "i" is a lava washer. They are self explanatory therefore no further description is needed.

The apparatus was calibrated by using Tl, Bi and Ce as calibration materials. Their transformation pressures are well established (1,2). The calibration points were double checked and showed a variation of less than 200 psi.

All electrical data were measured by a Rubicon potentiometer after equilibrium was established. Chromel and Alumel wires were used both as current and voltage leads and as thermocouples.

III. Results and Discussion

(1) SnTe Pressure-Temperature Phase Diagram Determination

It is well known that a phase transformation can be observed by measuring electrical resistance versus temperature or pressure. When the second phase is formed, the electrical resistance will show a sudden stepwise change.

From these phase transition data, a pressure-temperature phase diagram for SnTe, as shown in Fig. 2a, was constructed.

A closer examination of Fig. 2a, the P-T diagram of SnTe, reveals certain refinements or corrections which should be made. From the Clausius-Clapeyron equation, $dP/dT = \Delta S_{tr}/\Delta_{tr}$, where $\frac{dp}{dt}$ is the slope of the boundary line between two different phases, ΔS_{tr} is the entropy difference between the two different phases and ΔV_{tr} is the molar volume difference between the two different phases. The entropy change of our solid-solid transition should be less than that calculated from Richard's rule, $\Delta H_f/T_f = 2$ cal/deg. mole, since the rule applies to solid-liquid transitions. We can assume that ΔS_{tr} should be between 0.1 and 1 cal/deg. -mole.

For the reaction SnTe(I) → SnTe(II), ΔV is -14 cc/mole (3,4) and dP/dT should be between 0.3 and 3 atm/deg. However, the experimental value of $\frac{dP}{dT}$ from figure 2a is roughly 20 atm/deg. which is too high compared to our theoretical prediction. Therefore, the phase boundary between SnTe(I) and SnTe(II) in the neighborhood of room temperature should be more horizontal.

For the reaction SnTe(II) → SnTe(III), $\frac{dP}{dT}$ is observed to be roughly equal to 286 atm/deg. If ΔS is assumed to be between 0.1 and 1.0, then $\Delta V\ [V_{SnTe(III)} - V_{SnTe(II)}]$ must be roughly equal to 0.0145 to 0.145cc/mole. This means that $V_{SnTe(III)}$ is very slightly larger than and roughly equal to $V_{SnTe(II)}$.

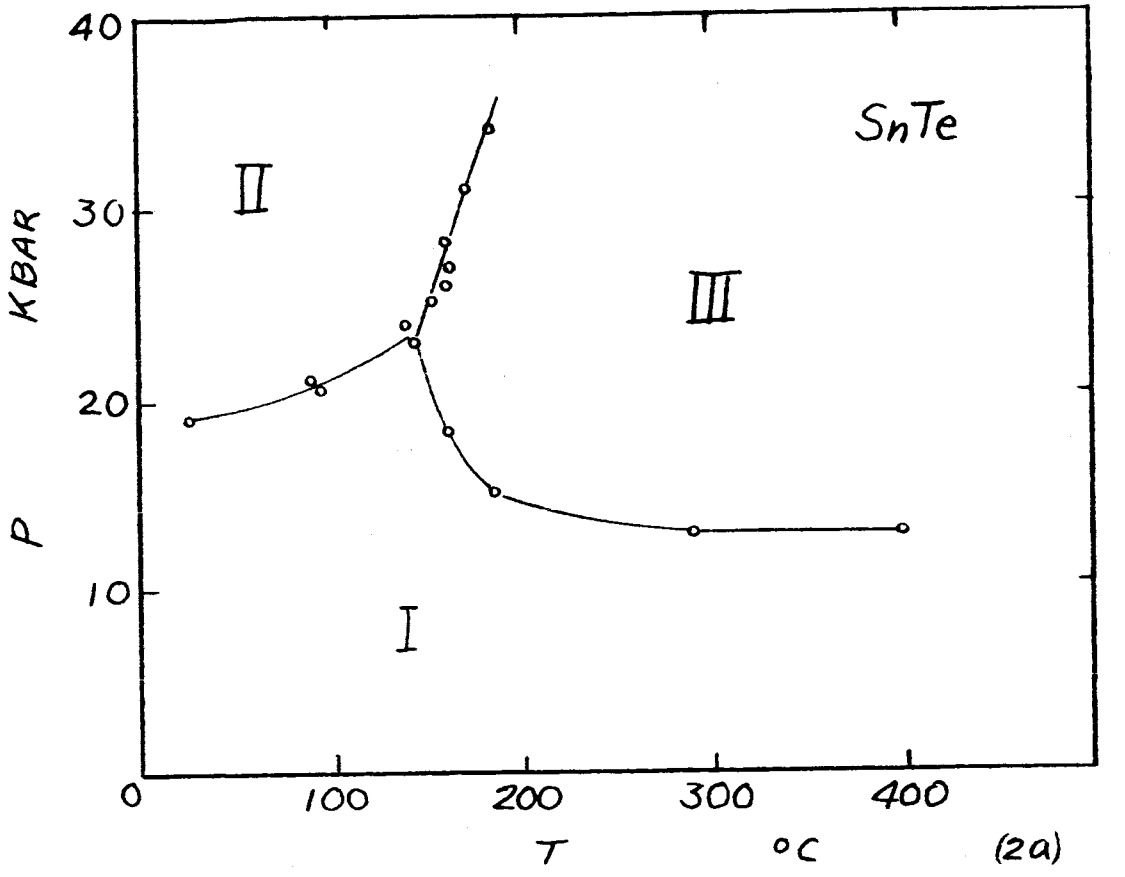

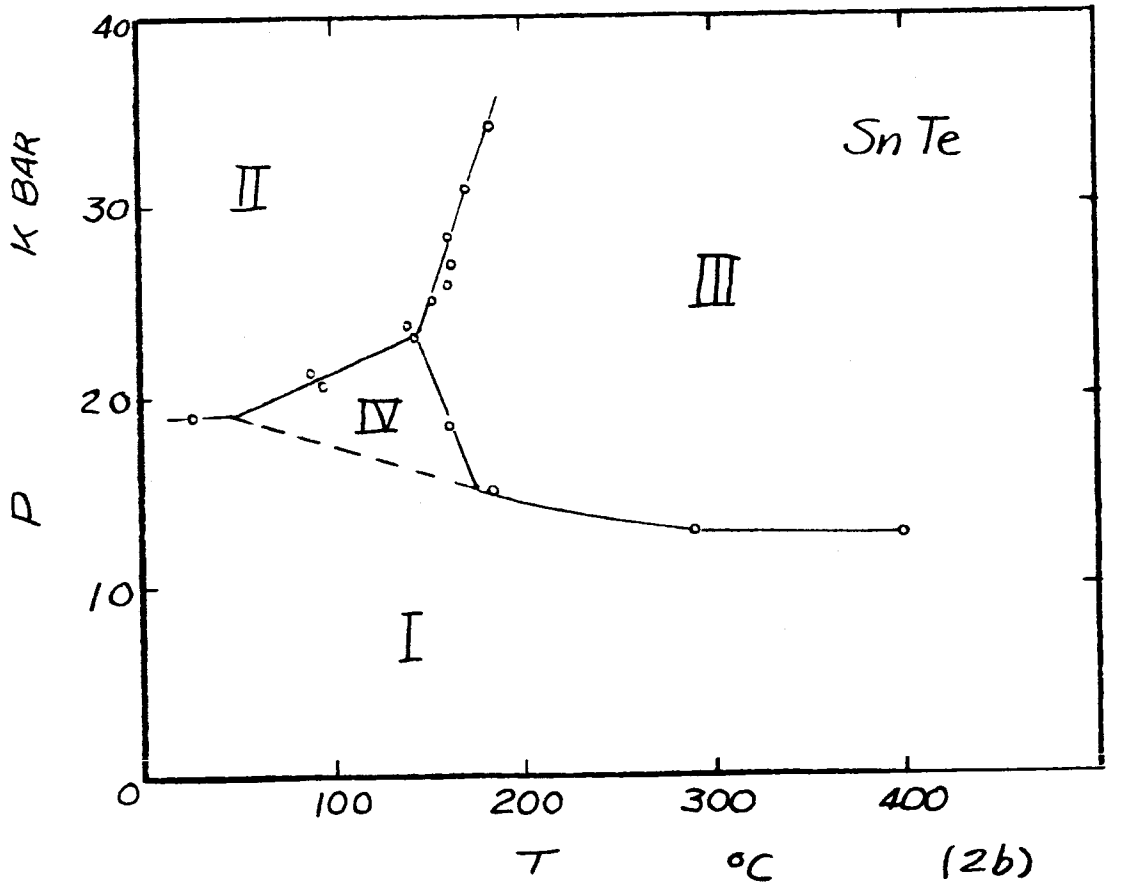

Figure 2 **P-T Diagram of SnTe**

The reaction SnTe(I) → SnTe(III) is approximately the same as the reaction SnTe(I) → SnTe(II). This means dP/dT should be almost horizontal which is what is observed.

Examining the reactions SnTe(I) → SnTe(II) and SnTe(I) → SnTe(III) near 140°C it is seen that the slope of $\frac{dP}{dT}$ is roughly equal to 50 and -280 atm/deg. respectively. In order to change $\frac{dP}{dT}$ from 3 to 50 or -3 to -280, we must reduce the ΔV about 15 or 90 times since ΔS cannot be increased over 2. Since these phase boundaries are at different temperatures and different pressures, we can consider the effects of thermal-expansion and compressibility. However, these coefficients are working against each other. Moreover, the coefficients are in the order of 10^{-5}/deg or -10^{-6}/atm, and within our temperature and pressure range, it is impossible to change the value of ΔV about 15 or 90 times. The conclusion from the above analysis is that the phase boundaries between SnTe(I) and SnTe(II) and between SnTe(I) and SnTe(III) in the neighborhood of 140°C are improbable as drawn. Such boundaries could exist only if there is another phase SnTe(IV) between SnTe(I), SnTe(II) and SnTe(III). We postulate that there is another phase SnTe(IV) situated under the triple point of SnTe(I), SnTe(II) and SnTe(III).

After these considerations, we construct a modified P-T diagram of SnTe as shown in Fig. 2b.

(2) E_g of SnTe(III)

When a material is in the intrinsic temperature range and it is assumed that there is no carrier generation other than that which results from thermal excitation of electrons and holes, the theoretical relationship between resistivity and temperature is

$$p = 2e\left(\frac{2\pi kT}{h^2}\right)^{\frac{3}{2}} (m_e m_h)^{-\frac{3}{4}} \exp\left(\frac{E_g}{2kT}\right)(\mu_e + \mu_h)^{-1}$$

where p is the resistivity, T is temperature in °K, E_g is the energy gap, μ_e and μ_h are the mobilities of the electrons and the holes, m_e and m_h are the effective masses of the electrons and the holes, e is the electrical charge, k is Boltzmann's constant and h is Planck's constant. This expression can be reduced to $p = B\exp\frac{E_g}{2KT}$ where B is constant if the mobility varies as $T^{\frac{-3}{2}}$. The above equation can be written in logarithmic form and differentiated to yield $d(\ln p) = \frac{E_g}{2k} d\left(\frac{1}{T}\right)$. The slope of the curve of log p vs $\frac{1}{T}$ is equal to $[(2.3)(2k)]^{-1}$ times the energy gap in the intrinsic temperature range.

The logarithm of resistivity as a function of reciprocal temperature is plotted in Fig. 3. SnTe(III) is found to have an energy gap of .28ev

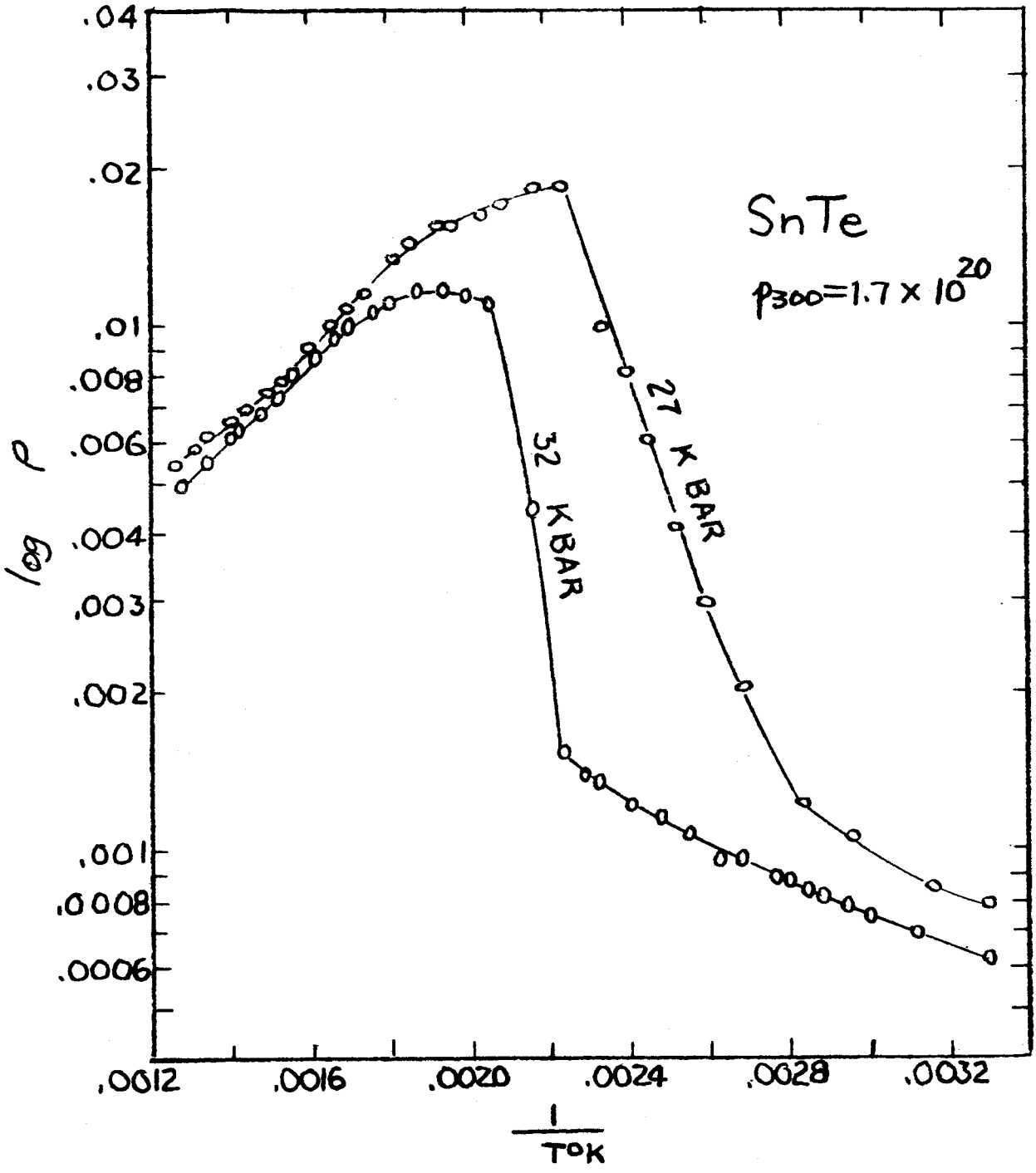

Figure 3 log p vs $\frac{1}{T}$

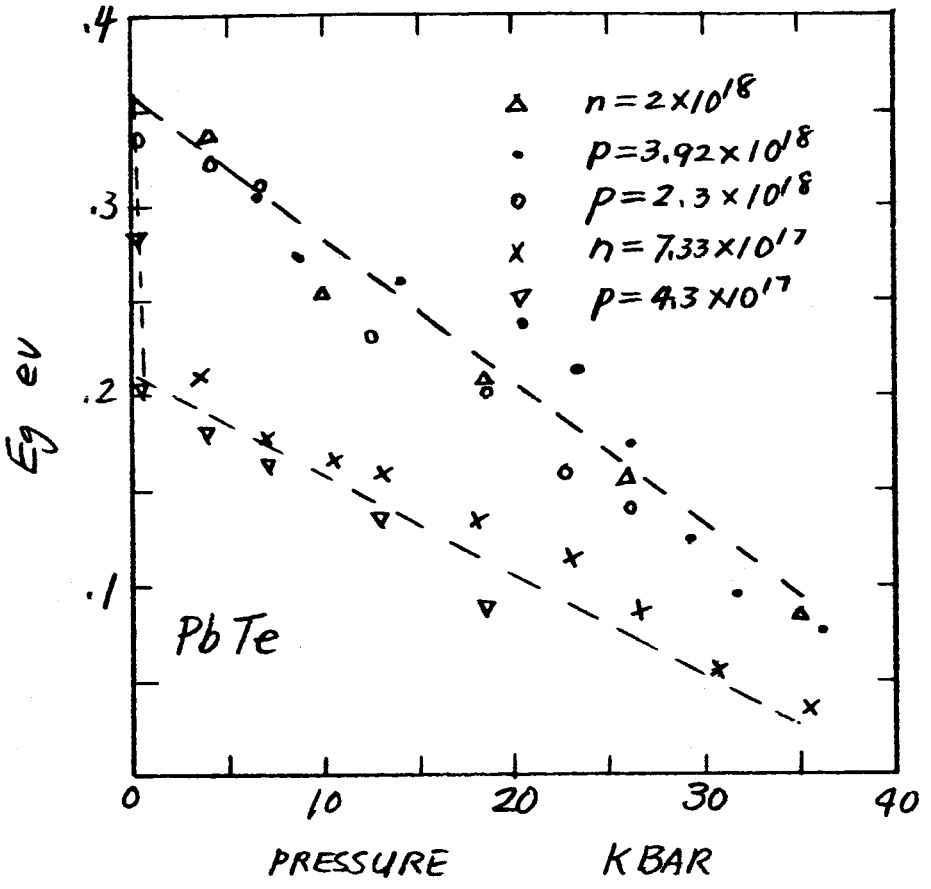

Figure 4 Eg vs P

at 32 kilobars. The effect of pressure on the energy gap is determined as $dE_g/dP = 7.75 \times 10^{-6}$ ev/atm in the pressure range of 28 to 32 kilobars.

(3) E_g of PbTe

Both n- and p-type PbTe were used as specimens, their carrier densities varied between $n = 7.33 \times 10^{17}$ cm^{-3} to $n \cong 2 \times 10^{18}$ cm^{-3} for the n-type and $p = 4.3 \times 10^{17}$cm^{-3} to $p = 3.92 \times 10^{18}$cm^{-3} for the p-type specimens.

An analysis similar to that for SnTe(III) can be applied to PbTe for the determination of E_g. Log p vs $\frac{1}{T}$ were plotted for these specimens at different pressures, and the E_g at these pressures were determined from the slopes of the plots. The data yielded an E_g and pressure relationship for these specimens and this is plotted in figure 4.

From Fig. 4, we noticed that there are two lines, one representing the high carrier density specimens 10^{18}cm^{-3} and the other the low carrier density specimens (10^{17}cm^{-3}). The high density carrier specimens showed a $\frac{dE_g}{dP} = -7.65 \times 10^{-6}$ev/atm and an E_g at atmospheric pressure equal to .36ev. These results are consistent with other investigations. However, the line which represents the 10^{17}cm^{-3} specimens showed low E_g values. Further investigation should be made to analyze this phenomenon. A possible explanation may be that there are two valence bands in the band structures of PbTe which has been suggested by recent infrared measurements (5). When the carrier density is low, we measured the optical energy gap between the conduction band and the first valence band which has been observed and measured using infrared absorption techniques. However, when the carrier density is high, we measured the gap between the conduction band and the second valence band usually obtained by suing the log resistivity versus $\frac{1}{T}$ plot.

IV. Conclusion

(1) P-T diagram of SnTe in the pressure range of atmospheric pressure to 35 kilobars and room temperature to 400°C has been determined.

(2) A high temperature and high pressure phase of SnTe(III) has been found.

(3) A fourth phase of SnTe situated between SnTe(I), SnTe(II) and SnTe(III) has been postulated from thermodynamic consideration.

(4) SnTe(III) shows semiconductor behavior with E_g = .28ev at 32 kilobars pressure

(5) dE_g/dP for SnTe(III) has been determined as 7.75×10^{-6} ev/atm.

(6) dE_g/dP for PbTe has been determined as -7.65×10^{-6} ev/atm.

V. Bibliography

1. Kennedy, G. C and La Mori, P.N.: "Prog. in Very High Pressure Research," John Wiley and Son, (1960).

2. Swenson, C. A.: "Solid State Physics," II, 99, (1960).

3. Hansen: "Constitution of Binary Alloys," McGraw-Hill, (1958).

4. Kafalas, J. A. and Mariano, A. N.: Science, 143, 952, (1964).

5. Tauber, R. T.: Thesis, N.Y.U., 1966.